Geophysical Research Letters

RESEARCH LETTER
10.1029/2024GL110622

Variations of Heat Flux and Elastic Thickness of Mercury From 3-D Thermal Evolution Modeling

Aymeric Fleury[1], Ana-Catalina Plesa[1], Nicola Tosi[1], Michaela Walterová[1,2], and Doris Breuer[1]

[1]German Aerospace Center (DLR), Institute of Planetary Research, Berlin, Germany, [2]Department of Geophysics, Faculty of Mathematics and Physics, Charles University, Prague, Czech Republic

Key Points:

- The distribution of Mercury's mantle temperature is strongly influenced by surface temperature and crustal thickness variations
- Surface heat flux and elastic thickness are controlled at large scales by surface temperature, and at small scales by crustal thickness
- Surface temperature variations influence the CMB heat flux distribution, which we make readily available to test dynamo models

Supporting Information:

Supporting Information may be found in the online version of this article.

Correspondence to:

A. Fleury,
aymeric.fleury@dlr.de

Citation:

Fleury, A., Plesa, A.-C., Tosi, N., Walterová, M., & Breuer, D. (2024). Variations of heat flux and elastic thickness of Mercury from 3-D thermal evolution modeling. *Geophysical Research Letters*, *51*, e2024GL110622. https://doi.org/10.1029/2024GL110622

Received 3 JUN 2024
Accepted 23 OCT 2024

Author Contributions:

Conceptualization: Ana-Catalina Plesa, Nicola Tosi, Michaela Walterová, Doris Breuer
Funding acquisition: Ana-Catalina Plesa
Investigation: Ana-Catalina Plesa, Nicola Tosi, Michaela Walterová, Doris Breuer
Methodology: Ana-Catalina Plesa, Nicola Tosi, Michaela Walterová
Software: Ana-Catalina Plesa, Nicola Tosi, Michaela Walterová
Supervision: Ana-Catalina Plesa
Writing – review & editing: Ana-Catalina Plesa, Nicola Tosi, Michaela Walterová, Doris Breuer

Abstract Mercury's low obliquity and 3:2 spin-orbit resonance create a surface temperature distribution with large latitudinal and longitudinal variations. These propagate via thermal conduction through the thin silicate shell influencing the interior temperature distribution. We use 3-D thermal evolution models to investigate the effects of lateral variations of surface temperature and crustal thickness on the surface and core-mantle boundary (CMB) heat fluxes, and elastic thickness distribution. Surface temperature variations cause a long-wavelength perturbation of the heat fluxes, as well as of the elastic lithosphere thickness, while variations in crustal thickness affect these quantities at small spatial scales. Like the surface temperature, the present-day CMB heat flux pattern is characterized primarily by spherical harmonics of degrees two and four, which could affect dynamo generation. Placing robust constraints on the thermal evolution based on the available estimates of the age and thickness of the elastic lithosphere remains challenging due to their large uncertainties.

Plain Language Summary The orbit of Mercury around the Sun leads to a specific surface temperature distribution, with some regions receiving more insolation than others. The thickness of Mercury's crust has been derived using gravity and topography data acquired by the MESSENGER mission. Since the rocky mantle of Mercury is rather thin (≈400 km), temperature variations driven by the insolation and by crustal properties (i.e., crustal heat sources and thermal conductivity) can affect the entire mantle, down to the core-mantle boundary. Here we model the global thermal evolution of Mercury, and investigate the influence of surface temperature and crustal thickness variations on the history and present-day state of the interior. We find that the surface temperature variations are reflected in the variations of Mercury's surface and core-mantle boundary heat fluxes, as well as in the thickness of the elastic part of its lithosphere. Crustal thickness variations lead to more local temperature differences, thus resulting in smaller scale variations in the lithosphere thickness and heat fluxes. The heat flux pattern at the core mantle boundary induced by the surface temperature distribution could affect magnetic field generation and should be tested by future dynamo models.

1. Introduction

Mercury's present-day spin rate is locked in a 3:2 resonance with the orbital motion. This configuration, combined with a relatively large orbital eccentricity and an almost perfect alignment of the spin axis with the orbit's normal, gives rise to a unique surface temperature pattern (Bauch et al., 2021; Paige et al., 1992, 2012; Vasavada et al., 1999). This pattern has a strong effect on surface processes as well as on lithospheric properties and thermal state of the interior (Tosi et al., 2015; Williams et al., 2011).

Besides surface temperature variations, crustal thickness variations influence the temperature distribution in the upper mantle as shown by Plesa et al. (2018) for Mars. In fact, the lower thermal conductivity of the crust compared to the mantle and its high enrichment in heat producing elements (HPE) lead to elevated subsurface temperatures at locations covered by thick crust. Upper mantle temperatures are decisive for estimating the elastic lithosphere thickness T_e (e.g., Grott & Breuer, 2008; Grott et al., 2013).

Estimates of the crustal thickness on Mercury were calculated from topography and gravity data collected by MESSENGER. With values of the average crustal thickness between 15 and 50 km (e.g., Padovan et al., 2015; Phillips et al., 2018; Smith et al., 2012; Sori, 2018), the volume of Mercury's crust represents about 6%–14% of the silicate volume, possibly the largest value among the terrestrial planets (Tosi & Padovan, 2021). Thus, information on Mercury's crustal thickness and its variations can be important upon assessing the thermal state of the interior.

Several studies investigated the thermal evolution and interior dynamics of Mercury using both 1-D parametrized (e.g., Grott et al., 2011; Hauck et al., 2004; Knibbe & Westrenen, 2018; Peterson et al., 2021; Tosi et al., 2013) and fully dynamical convection models (e.g., Guerrero et al., 2021; Michel et al., 2013; Padovan et al., 2017; Tosi et al., 2013). Tosi et al. (2015) used a combination of 3-D thermal and elastic models to show that the low-degree geoid and shape (at spherical harmonic degrees two and four) derived from MESSENGER can be explained in terms of the deformation caused by deep thermal anomalies induced by the present-day insolation pattern (see also Phillips et al., 2018). However, the influence of the insolation pattern on Mercury's interior dynamics and evolution has never been studied in detail and in particular in combination with lateral variations of the crustal thickness, which for Mercury can be significant (Beuthe et al., 2020a).

Here we use thermal evolution models in a 3-D spherical shell to determine the effects of surface temperature and crustal thickness variations on the heat fluxes and elastic lithosphere thickness of Mercury. We describe our methodology in Section 2 and present our results in Section 3. The main findings and their implications for the interpretation of forthcoming data from the BepiColombo mission are then discussed in Section 4. Conclusions are in Section 5.

2. Model

2.1. Thermal Evolution Model

We use the mantle convection code GAIA (Hüttig et al., 2013; Hüttig & Stemmer, 2008a, 2008b) in a 3-D spherical shell geometry. The conservation equations of mass, linear momentum, and thermal energy in the Extended Boussinesq Approximation (EBA) (Schubert et al., 2001; van Zelst et al., 2022) are available in the supplementary online information (Section S1 in Supporting Information S1).

We consider a temperature- and pressure-dependent viscosity that follows an Arrhenius law for diffusion creep. Core cooling is modeled by computing the temperature of the lower boundary according to a 1-D energy balance (Stevenson et al., 1983). While recent studies proposed a potential stratification of the core (Davies et al., 2024; Knibbe & Hoolst, 2021; Knibbe & Westrenen, 2018) which tends to keep the temperature of the CMB higher over time, here we assume an adiabatic core with constant density and heat capacity. In all models, we consider the decay of HPE using the heat sources concentrations from Table S1.1 in Supporting Information S1 and consider a higher heat production in the crust compared to the mantle (Plesa et al., 2015). A fixed concentration in HPE is assumed in the primitive mantle, which is then distributed between mantle and crust according to an enrichment factor λ set either at 1.61 or 10 (Table S1.1 in Supporting Information S1).

All our models consider the insulating effect of a low-conductivity crust that accounts for a 2 km-thick layer of megaregolith. A description of all parameters used in the models is available in Section S1 in Supporting Information S1.

2.2. Crustal Thickness Variations

In contrast to other thermal evolution models of Mercury, we include the effects of a laterally varying crustal thickness, similar to previous studies of the thermal evolution of Mars (Plesa et al., 2016, 2018). While this approach neglects crustal production and its associated effects on mantle composition, a process that might be important for the early stages of Mercury's evolution, it allows us to use the actual distribution of the crust, which otherwise would be impossible to reproduce self consistently. This implies that the crust was formed early on, and that variations in crustal thickness are assumed constant over time, which gives us the possibility to compare the thermal state of our models with local constraints. In our simulations, we use the crustal thickness maps of Beuthe et al. (2020a, 2020b), namely their models U0 (Figure 1a), V0 (Figure 1b), V3, and V4, that were inferred from the inversion of free-air gravity anomalies. The model U0 considers a homogeneous crustal density and an average crustal thickness of 35 km, while the V-models employ lateral variations of crustal density inferred from the mineralogy of the surface and the same average thickness of model U0. Among all models of Beuthe et al. (2020a), model V3 has the thinnest, while model V4 has the thickest average crust (25 and 45 km, respectively). A complete description of the crustal thickness models is available in Section S5 in Supporting Information S1.

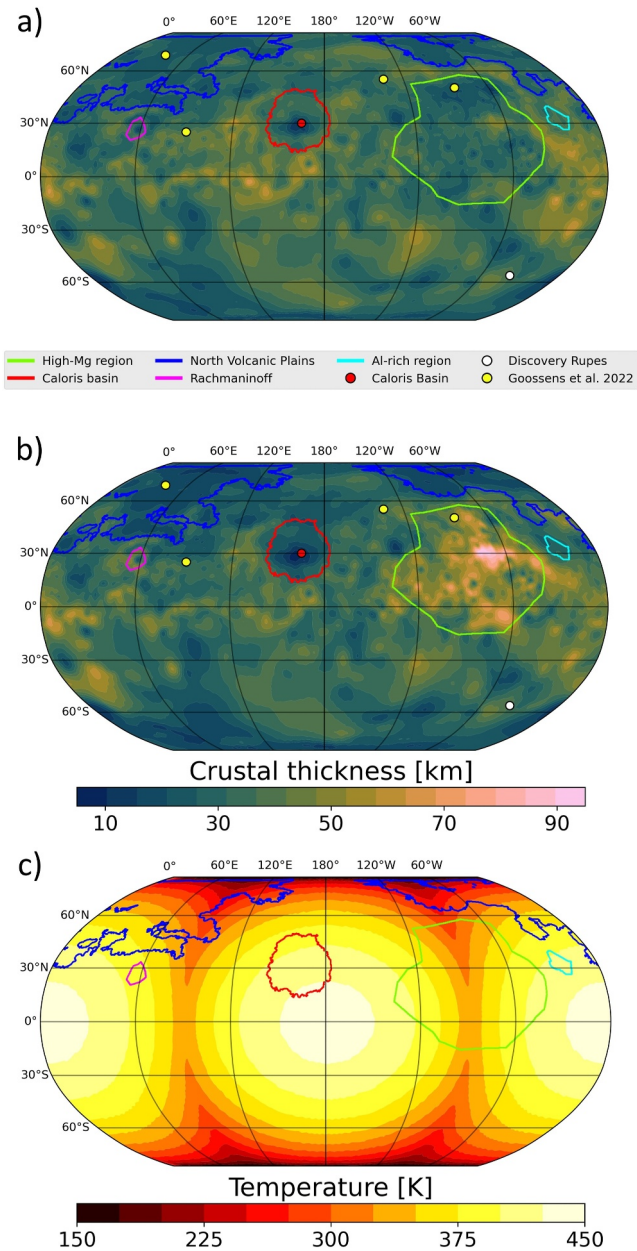

Figure 1. (a) Crustal thickness distribution from model U0 (Beuthe et al., 2020a) with a laterally uniform crustal density, and an average thickness of 35 km (b) Crustal thickness distribution from model V0 (Beuthe et al., 2020a) with a laterally variable crustal density, and an average thickness of 35 km. Colored lines indicate different geochemical terrains and geological features (Weider et al., 2015): High-Mg region, Northern Volcanic Plains (NVP), Caloris and Rachmaninoff basins, Al-rich region. The dots show other locations of interest for which estimates of elastic lithosphere thickness are available (Goossens et al., 2022). (c) Average surface temperature distribution. The maps are shown in Robinson projection centered at 180°E.

2.3. Surface Temperature Variations

In addition to the crustal thickness variations, we also consider surface temperature variations. Because of its very low obliquity, Mercury experiences significant temperature variations between the polar and equatorial regions (Margot et al., 2012). Furthermore, the 3:2 spin-orbit resonance and a relatively large orbital eccentricity give rise to significant longitudinal temperature variations (Siegler et al., 2013; Vasavada et al., 1999). The coexistence of these two effects creates a peculiar surface temperature distribution with two equatorial hot poles and two latitudinal cold poles (Figure 1c). In between the hot poles, two equatorial warm poles are located around 90°E and 90°W longitudes.

In our models, we use this temperature distribution as a surface boundary condition throughout the evolution (see Figure 1c) assuming that the present-day 3:2 spin-orbit resonance was acquired early and that the obliquity and orbital eccentricity have not changed considerably. Other studies have suggested that Mercury's current spin state may have been acquired relatively late in the evolution, after the Caloris-forming impact (Wieczorek et al., 2012). Before this event, Mercury may have maintained different resonances such as 1:1 or 2:1, which are more consistent with the distribution of pre-Calorian basins (Knibbe & Westrenen, 2017; Wieczorek et al., 2012). Furthermore, orbital eccentricity might have been varying under the influence of other planets (Laskar & Gastineau, 2009). Nevertheless, combined orbital and rotational evolution models also suggest that Mercury may have been captured into its current 3:2 resonance within a few tens of million years, thus justifying our assumption on the spin rate (Noyelles et al., 2014).

2.4. Elastic Thickness Calculations

We use our thermal evolution models to calculate the elastic lithosphere thickness through time. To this end, we employ the Conversion $T - T_e$ package from Broquet (2022) using, at each location on the planet's surface, the corresponding local temperature profile and a prescribed rheology. In addition, we assume a flexural curvature of 5×10^{-7} m^{-1} (Katayama, 2021; McNutt, 1984; Nimmo & Watters, 2004; Zuber et al., 2012). The $T - T_e$ package relies on the strength envelope formalism of McNutt (1984) and considers a two-layer model of crust and mantle. The brittle-strength envelopes are calculated according to Mueller and Phillips (1995). We refer to Section S3 in Supporting Information S1 for an in-depth description. Here, we focus on the time evolution of the elastic thickness for six regions, namely the Caloris Basin, the Discovery Rupes scarp, and four additional locations recently studied by Goossens et al. (2022).

3. Results

3.1. Surface and CMB Heat Flux

The surface temperature distribution imposes a long-wavelength pattern on the present-day CMB and surface heat fluxes, independent of the choice of the crustal thickness model (left and central columns in Figure 2). The heat flux is highest at the two geographic poles and around the two longitudinal low-temperature bands, and lowest around the two equatorial hot poles (Figures 2a–2c). Crustal thickness variations locally modify the heat flux distribution (cf. surface and CMB heat flux maps for the crustal thickness models U0, V0, and V4 in Figure 2). The positive thermal anomalies induced by the combination of the hot poles and increased crustal thickness propagate through the entire mantle and heat up locally the CMB. The impact of the crustal thickness on the heat flux variations depends on the crustal

10.1029/2024GL110622

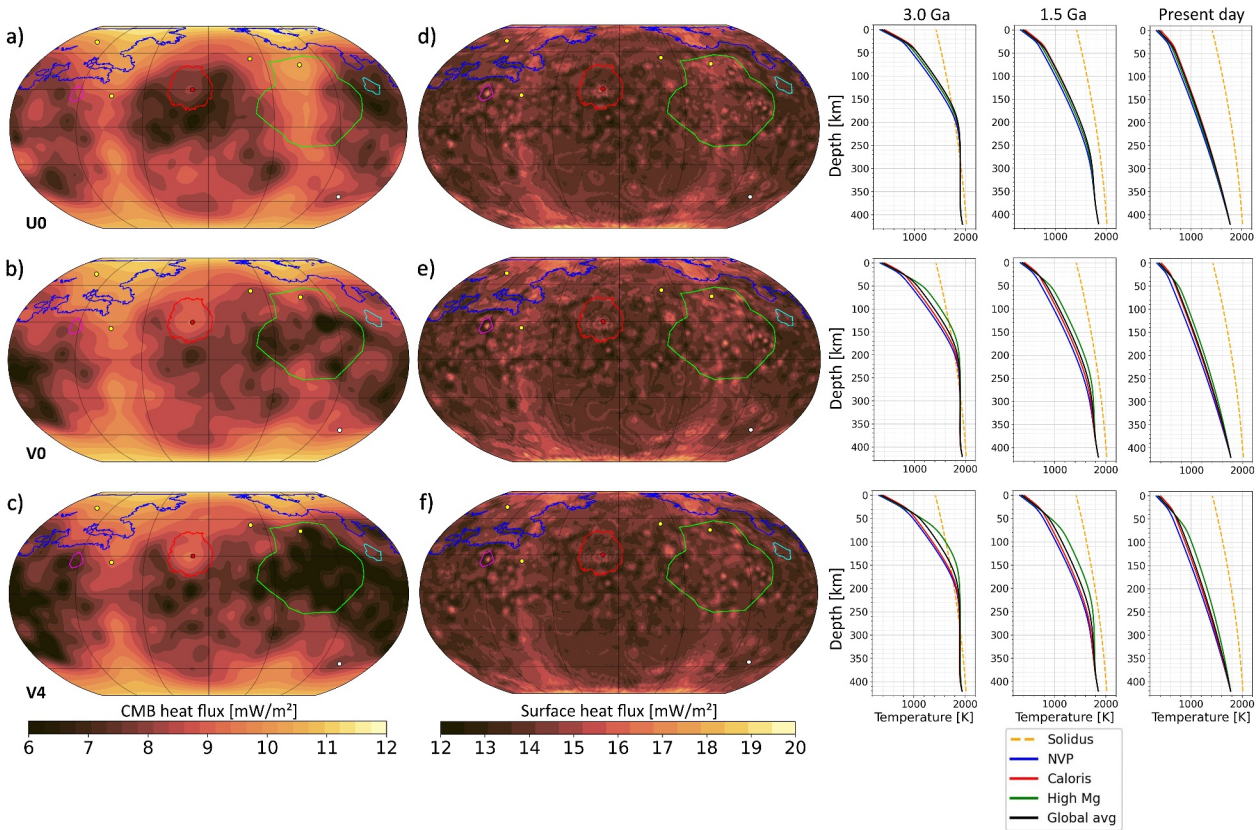

Figure 2. Maps of the heat fluxes at the CMB (a)–(c) and surface (d)–(f) of Mercury at present day. The maps correspond to different crustal models of Beuthe et al. (2020a): U0 (a, d), V0 (b, e), and V4 (c, f). All models use a crustal enrichment in HPE of 1.61 and an initial temperature of 1,800 k. The maps use a Robinson projection centered at 180°E, with colored lines and dots indicating regions of interest (see Figure 1). The color bars for the heat flux maps are saturated for improved readability. The right column shows temperature profiles for the NVP region, Caloris basin, High-Mg region, and global average at different times. The dashed yellow line shows the solidus temperature from Namur et al. (2016).

enrichment, becoming more accentuated for a higher enrichment in HPE (see Figures S8.2 and S8.3 in Supporting Information S1).

The cases with variable density crusts (V-cases in Figure 2) show a thicker crust in the High-Mg region, for which a lower CMB heat flux is observed when compared to the case with a constant density crust (case U0 in Figure 2). Only cases with $\lambda = 10$ show a noticeably higher surface heat flux in the areas covered by a thicker crust (Figures S8.2e,f and S8.3e,f in Supporting Information S1). Contrarily to regions covered by a thick crust, areas corresponding to a thin crust such as the Northern Volcanic Plains (NVP), the south pole, the Caloris basin, and the Rachmaninoff basin show an increased heat flux at the CMB.

In simulations with a low crustal enrichment ($\lambda = 1.61$), remnants of the small mantle convection cells can still be observed at present day in some areas on the map of the CMB heat flux (Figure 2, left column). This pattern is however less pronounced in simulations with a higher crustal enrichment ($\lambda = 10$, Figures S8.2 and S8.3 in Supporting Information S1), as the more depleted mantle cannot sustain convection until present day. On average, the mantle transitions from a convective state to a conductive state between 3 and 3.5 Gyr (see Section S5 in Supporting Information S1). In this case, the local temperature anomalies induced by the crustal thickness variations are much stronger than those due to mantle plumes. For a detailed description of the present-day temperature distribution of each simulation, we refer the reader to Figure S8.4 in Supporting Information S1.

In addition to the surface and CMB heat flux maps, Figure 2 also shows temperature profiles at specific locations (NVP region, Caloris basin, High-Mg region), laterally averaged within the bounding contour, in comparison to the global average temperature profile at different times during the evolution. As a reference, we also show the lherzolite solidus proposed by Namur et al. (2016), which is appropriate for Mercury's bulk mantle. Since we

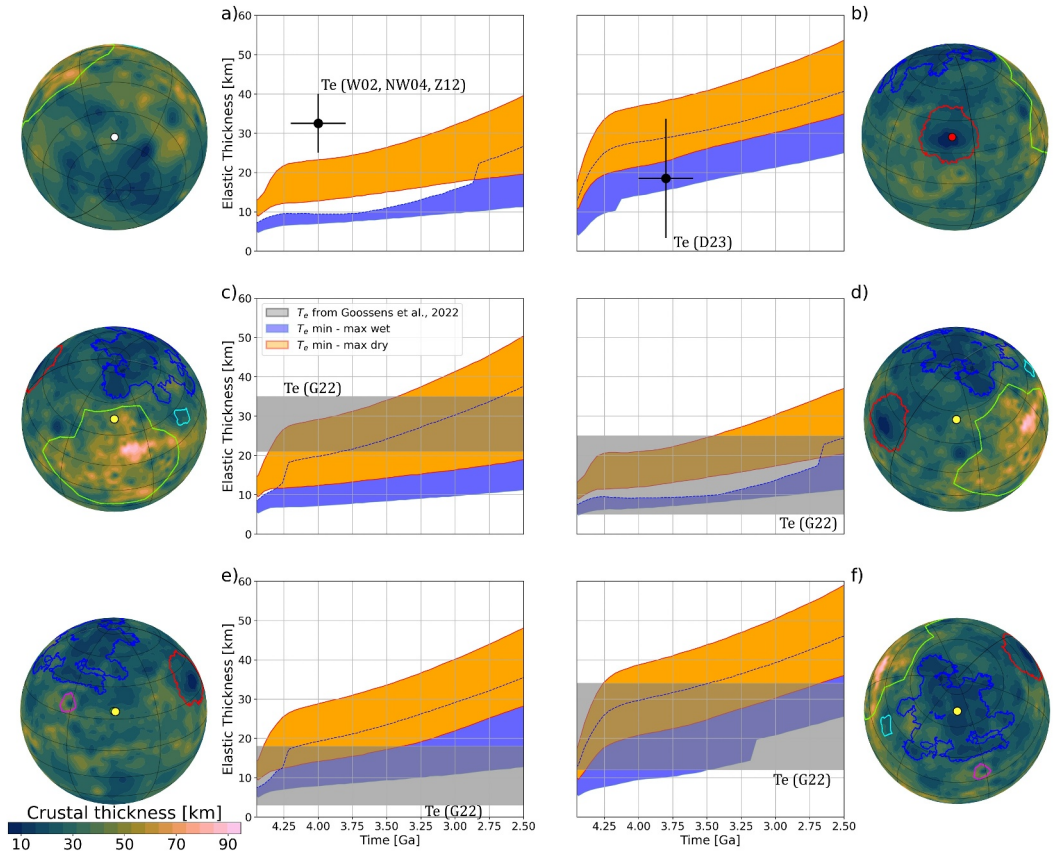

Figure 3. Evolution of the elastic lithosphere thickness of different areas and comparison with literature estimates: W02 - Watters et al. (2002); NW04 - Nimmo and Watters (2004); Z12 - Zuber et al. (2012); G22 - Goossens et al. (2022); D23 - Deng et al. (2023). The panels show the entire range of values obtained from all simulations (U0, V0, V3, and V4 models) for a dry rheology (orange) and a wet rheology (blue). The blue dashed line shows the maximum values of elastic thickness with a wet rheology that sometimes overlap with those obtained with a dry rheology. Next to each time evolution panel, we show the location of the corresponding zone indicated by a colored point on an Orthographic projection of the crustal model V0 of Beuthe et al. (2020a). The investigated areas are: (a) Discovery Rupes, (b) Caloris Basin, (c) Goossens point N°1 (85°W, 50°N), (d) Goossens point N°2 (135°W, 55°N), (e) Goossens point N°3 (90°E, 25°N), and (f) Goossens point N°4 (40°E, 70°N). Solid colored lines indicate different geochemical terrains (Weider et al., 2015).

assume that the whole crust was emplaced early on, this solidus only provides a lower bound. We observe a clear difference between the thermal state at different geological locations, in particular for models that use a variable crustal density, which leads to stronger crustal thickness variations. In these models the highest temperature is obtained in the High-Mg region that is covered by a thick crust, while the thin NVP crust leads to the coldest thermal profile throughout the evolution.

3.2. Elastic Thickness

We compare the evolution of the elastic lithosphere thickness (T_e) from our models at specific locations where literature estimates exist based on the analysis of local gravity and topography data (e.g., Goossens et al., 2022; Phillips et al., 2018). Our results indicate a general trend across all locations: as the planet cools, the elastic lithosphere thickness increases as shown in Figure 3. Given that the regions we study are relatively ancient, we have limited our analysis of the elastic thickness evolution to the first two billion years. We modeled the elastic thickness assuming either a wet or a dry crust and mantle rheology, shown as blue and orange envelopes in Figure 3, respectively.

The elastic thickness estimates for the Discovery Rupes scarp range between 25 and 40 km at the time of its formation around 4 ± 0.2 Ga (Nimmo & Watters, 2004; Watters et al., 2002; Zuber et al., 2012). Our models,

however, show values of less than 10 km for a wet rheology and up to 23 km for a dry rheology, the latter aligning better with the lower end of the literature estimates (Figure 3a).

For the Caloris Basin, our models are in good agreement with the most recent estimate from Deng et al. (2023) between 3.3 and 33.7 km. These estimates were inferred using an admittance function derived from the most recent topography and gravimetry data.

Although Goossens et al. (2022) do not specify exact times for their estimates, they suggest that their findings likely represent the period between 4.2 and 3.5 Ga. Our models show a good match if the elastic thickness for these regions is associated with an early time of formation. Despite uncertainties in both time and measured thickness, we cannot definitively favor models using either a wet or dry rheology, although the results seem to be better compatible with a wet rheology.

Figure 4 displays the global evolution of the elastic lithosphere thickness from all models, assuming both a dry (orange envelope) and a wet rheology (blue envelope). The calculation of the elastic thickness is based on the minimum and maximum temperature profiles of each simulation, different to Figure 3, where only the local temperature profiles were used. Additionally, maps showing the elastic thickness and thermal profiles at various times, using the crustal thickness model V0, are depicted. Similar to the present-day heat fluxes (Figure 2), the surface temperature induces a predominant degree-2 distribution with large elastic thickness at the geographical poles and smaller thickness at the two equatorial hot poles throughout the evolution. The crustal thickness distribution leads to smaller scale modifications of the elastic thickness, as zones covered by a thin crust outline areas with large lithospheric thickness.

The evolution of the temperature profiles, laterally averaged over three different geochemical terrains (Weider et al., 2015), namely NVP, High-Mg region, and the Caloris basin, indicates that these regions have experienced distinct thermal histories (Figures 2 and 4). In particular the simulations with a variable crustal density show the largest differences in the thermal profiles. When comparing these thermal profiles at present-day, we note a temperature difference of up to 200 K between the NVP and the High-Mg region (Figures 2 and 4, Figures S8.1, S8.2, and S8.3 in Supporting Information S1) at a depth of 100 km for the most extreme cases.

4. Discussion

The temperature resulting from the 3:2 spin-orbit resonance has a strong effect on both the surface and CMB heat fluxes. While the average surface heat flux varies by less than 1 mW m^{-2} between the models, the insolation pattern and the crustal thickness variations lead to a clear difference in the local heat fluxes and temperature profiles throughout the thermal history. Previous studies have investigated the surface composition of the northern hemisphere of Mercury and identified several geochemically distinct terrains (Peplowski et al., 2015; Weider et al., 2015), which might be associated with mantle regions that experienced distinct thermal and magmatic histories. Simulations using variable density crusts indicate the presence of a persistent positive thermal anomaly beneath the High Mg-region, lasting until present (see Figure S8.4 in Supporting Information S1). Indeed, this region was likely generated during the early stages of Mercury's evolution by high-degree partial melting (Beuthe et al., 2020a; Namur et al., 2016; Wang et al., 2022), hence by an anomalously hot mantle that may have left a long-lasting thermal signature.

Despite the simplified treatment of core cooling, our models predict an average CMB heat flux that exceeds the core adiabatic heat flux up to approximately 0.5 Gyr (see Section S5 in Supporting Information S1), supporting the idea of an early thermal dynamo. To assess the feasibility of the present-day dynamo, a more sophisticated model of core cooling and crystallization would be required (Davies et al., 2024; Knibbe & Westrenen, 2018). In particular, the formation of a thermally stratified layer at the top of the core could slow down the evolution of the CMB temperature. Although the full implications for our results remain to be assessed, we do not expect the CMB heat flux patterns to be significantly affected.

Recent dynamo models have investigated the role of a heterogeneous CMB heat flux pattern in reproducing Mercury's magnetic field. Tian et al. (2015) successfully produced Mercury-like magnetic fields using dynamo models that incorporated a degree-1 spherical harmonic, north-south asymmetric heat flux at the CMB. An alternative CMB heat flux pattern, characterized by spherical harmonics of degree two and four, has been proposed by Cao et al. (2014) to explain the hemispheric field of Mercury. However, their model exhibits the highest heat flow at the equator, opposite to what our models indicate when considering the surface temperature and

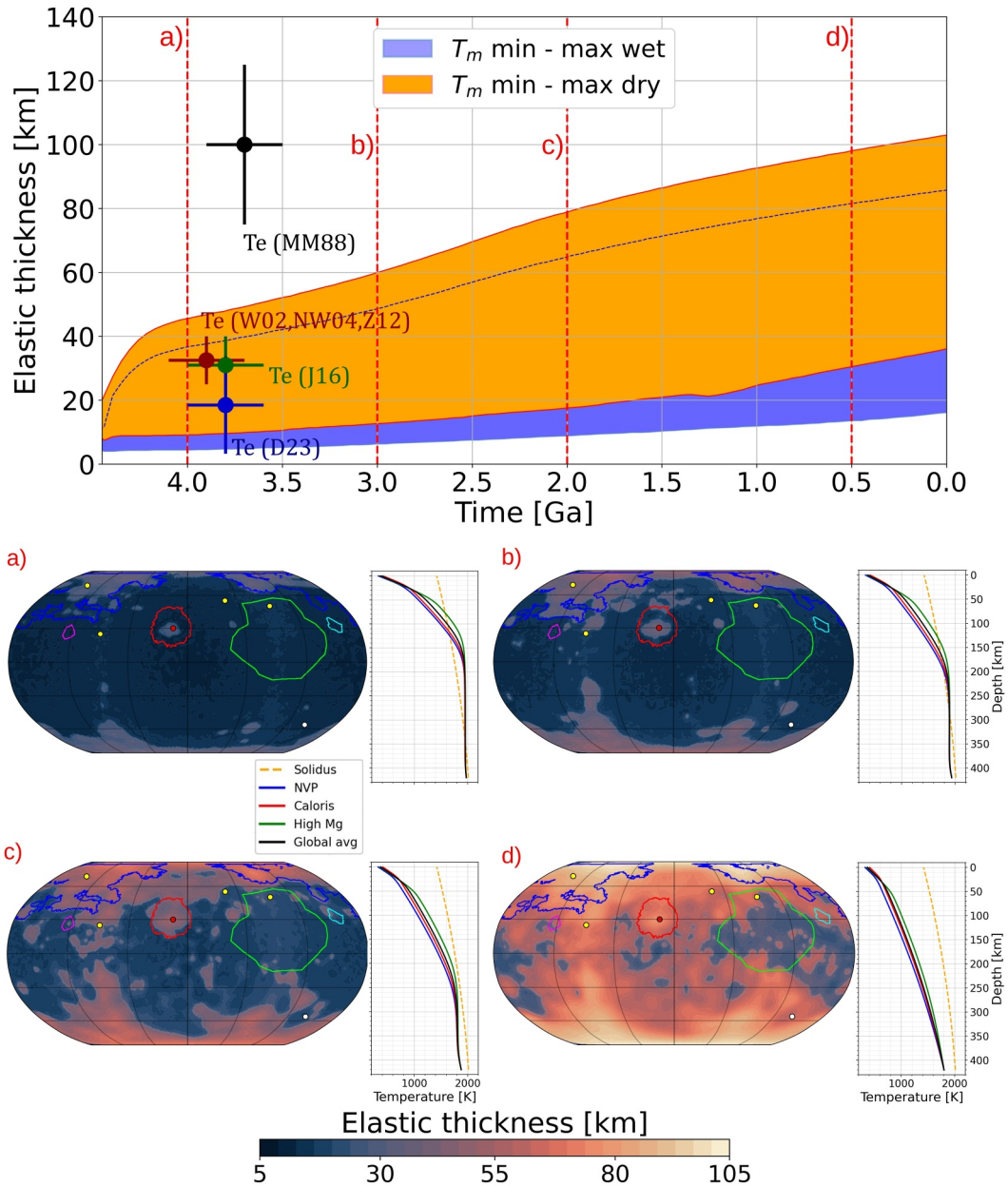

Figure 4. Evolution of the elastic lithosphere thickness assuming a dry (orange envelope) and wet rheology (blue envelope) for all models and for every location on the planet. The symbols indicate values from MM88 - Melosh and McKinnon (1988); W02 - Watters et al. (2002); NW04 - Nimmo and Watters (2004); Z12 - Zuber et al. (2012); and J16 - James et al. (2016). The two estimates MM88 and D23 relate to the Caloris Basin, whereas the J16 estimate applies to the northern hemisphere. Global elastic lithosphere thickness maps show spatial variations at different times: (a) 4 Ga, (b) 3 Ga (c) 1.5 Ga, and (d) 0.5 Ga using the crustal model V0 (Beuthe et al., 2020a). The color scale is saturated at minimum and maximum values of 5.9 and 116 km, respectively. Temperature profiles for the NVP region, Caloris basin, High-Mg region, and global average are displayed at the respective times during the evolution. The solidus (yellow dashed line) is shown for reference. All maps use a Robinson projection and colored lines indicate different geochemical terrains (Weider et al., 2015).

crustal thickness variations. Future studies should investigate the consequences of the CMB heat flux pattern obtained in this work on Mercury's magnetic field. For this purpose, we used the SHTOOLS software package (Wieczorek & Meschede, 2018) and provide 4π-normalized spherical harmonics coefficients for the CMB heat flux from all our models in the SI.

The elastic lithospheric thickness calculation is particularly dependent on the considered flexural curvature, as previous studies showed (Katayama et al., 2019; McNutt, 1984). Local flexural curvature may vary strongly among geological features depending on their respective tectonic context. In this study, we chose a curvature of $K = 5 \times 10^{-7}$ m^{-1}, a value typically used in the literature (e.g., Katayama, 2021; Nimmo & Watters, 2004). We note that not all locations studied here are associated with specific geological features, and thus, flexural curvature estimates are not always available. We decided to use the same flexural curvature for all locations in order to have a better comparison between the estimates. We acknowledge, however, that the value of the flexural curvature has a first order impact on the elastic thickness estimates and show the effects for various values proposed for the Caloris Basin (Figure S6.1 in Supporting Information S1).

The estimates of the elastic thickness currently available in the literature do not allow us to robustly constrain the parameters controlling Mercury's thermal evolution. Better information on the possible time of loading (i.e., the time at which T_e was "frozen in") associated with the locations of the elastic thickness estimates studied here would help constrain the thermal state of the subsurface and potentially exclude some of the models we presented. Future data from BepiColombo for the southern hemisphere to better characterize contractional landforms could help to further constrain the depth of the brittle-ductile transition, similar to what has been done for Discovery Rupes (Nimmo & Watters, 2004; Williams et al., 2011).

Finally, the lateral temperature variations that we determined would affect not only the viscosity, but also other temperature-dependent parameters of the mantle such as rigidity and bulk modulus. Lateral changes in these quantities could affect tidal deformation to the extent of being potentially detectable by BepiColombo (Rovira-Navarro et al., 2024), suggesting that our models could also provide a baseline for future models of tidal response based on 3D structures.

5. Conclusions

We investigated the effects of spatial variations of both crustal thickness and surface temperature on the evolution and present-day thermal state of the interior of Mercury. We have shown that the thermal evolution of Mercury's mantle is strongly influenced by the insolation pattern and by the distribution of the crustal thickness. The surface temperature distribution creates a long-wavelength pattern on both the heat fluxes and on the elastic lithospheric thickness. Additionally, crustal thickness variations induce smaller scale variations on the two quantities.

We provide the most detailed distribution of the present-day CMB heat flux of Mercury based on a self-consistent thermal evolution model. Such a distribution should be tested in future dynamo models. Our models also suggest that different geochemical terrains, such as the NVP and the High Mg-Region, could have experienced different thermal histories throughout the evolution, owing to their different crustal thicknesses and surface location.

Future data from BepiColombo (Benkhoff et al., 2021) will provide a better resolution for the gravity and topography of Mercury, as well as measurements of its surface composition. These new data will help refine the estimates of the elastic lithosphere thickness that can be used to constrain our thermal evolution models and improve our understanding of the thermal history and present-day state of Mercury's interior.

Data Availability Statement

All data presented in this paper is available in tabulated form on Zenodo (Fleury et al., 2024). The GAIA code is a proprietary code of DLR. Users interested in working with it should contact Ana-Catalina Plesa (ana.plesa@dlr.de) and Christian Hüttig (christian.huettig@dlr.de).

Acknowledgments

A.F and A.C.P. gratefully acknowledge the financial support and endorsement from the DLR Management Board Young Research Group Leader Program and the Executive Board Member for Space Research and Technology. M.W. has been supported by the Czech Science Foundation Grant 23-06513I. We thank two anonymous reviewers for their thoughtful comments, which helped improve an earlier version of this paper and the editor Kevin Lewis for handling our manuscript. In particular, we warmly thank one of the reviewers for thoroughly checking the supporting data sets and providing comments that helped to improve their usability. We thank the BELA Experiment teams at DLR (Institute of Planetary Research, Berlin) and at University of Bern (Physikalisches Institut, Bern) as well as the BELA Science Team. We also acknowledge the support by the BepiColombo project teams at ESTEC, ESOC, and ESAC. Open Access funding enabled and organized by Projekt DEAL.

References

Bauch, K. E., Hiesinger, H., Greenhagen, B. T., & Helbert, J. (2021). Estimation of surface temperatures on Mercury in preparation of the MERTIS experiment onboard BepiColombo. *Icarus*, *354*, 114083. https://doi.org/10.1016/j.icarus.2020.114083

Benkhoff, J., Murakami, G., Baumjohann, W., Besse, S., Bunce, E., Casale, M., et al. (2021). Bepicolombo - Mission overview and science goals. *Space Science Reviews*, *217*(8), 90. https://doi.org/10.1007/s11214-021-00861-4

Beuthe, M., Charlier, B., Namur, O., Rivoldini, A., & Van Hoolst, T. (2020a). Mercury's crustal thickness correlates with lateral variations in mantle melt production. *Geophysical Research Letters*, *47*(9), e2020GL087261. https://doi.org/10.1029/2020GL087261

Beuthe, M., Charlier, B., Namur, O., Rivoldini, A., & Van Hoolst, T. (2020b). Mercury's crustal thickness correlates with lateral variations in mantle melt production: Dataset for maps of surface density, degree of partial melting, and crustal thickness. *Zenodo*. https://doi.org/10.5281/zenodo.3727115

Broquet, A. (2022). Ab-ares/te_hf_conversion: 0.2.3. *Zenodo*. [Software]. https://doi.org/10.5281/zenodo.6050262
Cao, H., Aurnou, J. M., Wicht, J., Dietrich, W., Soderlund, K. M., & Russell, C. T. (2014). A dynamo explanation for Mercury's anomalous magnetic field. *Geophysical Research Letters*, *41*(12), 4127–4134. https://doi.org/10.1002/2014GL060196
Davies, C. J., Pommier, A., Greenwood, S., & Wilson, A. (2024). Thermal and magnetic evolution of mercury with a layered fe-si(-s) core. *Earth and Planetary Science Letters*, *641*, 118812. https://doi.org/10.1016/j.epsl.2024.118812
Deng, Q., Xiao, Z., Zhong, Z., Ye, M., Li, F., Yan, J., & Barriot, J.-P. (2023). Lithospheric elastic thickness beneath the Caloris Basin: Implications for the thermal structure of mercury. *Journal of Geophysical Research: Planets*, *128*(5), e2023JE007796. https://doi.org/10.1029/2023JE007796
Fleury, A., Plesa, A.-C., Tosi, N., Walterova, M., & Breuer, D. (2024). Datasets concerning variations of heat flux and elastic thickness of mercury from thermal evolution modeling. *Zenodo*. [Dataset]. https://doi.org/10.5281/zenodo.11402214
Goossens, S., Genova, A., James, P. B., & Mazarico, E. (2022). Estimation of crust and lithospheric properties for mercury from high-resolution gravity and topography. *The Planetary Science Journal*, *3*(6), 145. https://doi.org/10.3847/PSJ/ac703f
Grott, M., Baratoux, D., Hauber, E., Sautter, V., Mustard, J., Gasnault, O., et al. (2013). Long-term evolution of the martian crust-mantle system. *Space Science Reviews*, *172*(1), 49–111. https://doi.org/10.1007/s11214-012-9948-3
Grott, M., & Breuer, D. (2008). The evolution of the Martian elastic lithosphere and implications for crustal and mantle rheology. *Icarus*, *193*(2), 503–515. https://doi.org/10.1016/j.icarus.2007.08.015
Grott, M., Breuer, D., & Laneuville, M. (2011). Thermo-chemical evolution and global contraction of Mercury. *Earth and Planetary Science Letters*, *307*(1), 135–146. https://doi.org/10.1016/j.epsl.2011.04.040
Guerrero, J. M., Lowman, J. P., & Tackley, P. J. (2021). Did the cessation of convection in Mercury's mantle allow for a dynamo supporting increase in heat loss from its core? *Earth and Planetary Science Letters*, *571*, 117108. https://doi.org/10.1016/j.epsl.2021.117108
Hauck, S. A., Dombard, A. J., Phillips, R. J., & Solomon, S. C. (2004). Internal and tectonic evolution of Mercury. *Earth and Planetary Science Letters*, *222*(3), 713–728. https://doi.org/10.1016/j.epsl.2004.03.037
Hüttig, C., & Stemmer, K. (2008a). Finite volume discretization for dynamic viscosities on Voronoi grids. *Physics of the Earth and Planetary Interiors*, *171*(1–4), 137–146. https://doi.org/10.1016/j.pepi.2008.07.007
Hüttig, C., & Stemmer, K. (2008b). The spiral grid: A new approach to discretize the sphere and its application to mantle convection. *Geochemistry, Geophysics, Geosystems*, *9*(2), Q02018. https://doi.org/10.1029/2007GC001581
Hüttig, C., Tosi, N., & Moore, W. B. (2013). An improved formulation of the incompressible Navier-Stokes equations with variable viscosity. *Physics of the Earth and Planetary Interiors*, *40*, 113–129. https://doi.org/10.1016/j.pepi.2013.04.002
James, P., Phillips, R., Grott, M., Hauck, S., & Solomon, S. (2016). The thickness of Mercury's lithosphere inferred from MESSENGER gravity and topography.
Katayama, I. (2021). Strength models of the terrestrial planets and implications for their lithospheric structure and evolution. *Progress in Earth and Planetary Science*, *8*(1), 1–17. https://doi.org/10.1186/s40645-020-00388-2
Katayama, I., Matsuoka, Y., & Azuma, S. (2019). Sensitivity of elastic thickness to water in the Martian lithosphere. *Progress in Earth and Planetary Science*, *6*(1), 51. https://doi.org/10.1186/s40645-019-0298-6
Knibbe, J., & Van Hoolst, T. (2021). Modelling of thermal stratification at the top of a planetary core: Application to the cores of earth and mercury and the thermal coupling with their mantles. *Physics of the Earth and Planetary Interiors*, *321*, 106804. https://doi.org/10.1016/j.pepi.2021.106804
Knibbe, J., & van Westrenen, W. (2017). On mercury's past rotation, in light of its large craters. *Icarus*, *281*, 1–18. https://doi.org/10.1016/j.icarus.2016.08.036
Knibbe, J., & van Westrenen, W. (2018). The thermal evolution of mercury's fe–si core. *Earth and Planetary Science Letters*, *482*, 147–159. https://doi.org/10.1016/j.epsl.2017.11.006
Laskar, J., & Gastineau, M. (2009). Existence of collisional trajectories of mercury, mars and venus with the earth. *Nature*, *459*(7248), 817–819. https://doi.org/10.1038/nature08096
Margot, J. L., Peale, S. J., Solomon, S. C., Hauck II, S. A., Ghigo, F. D., Jurgens, R. F., et al. (2012). Mercury's moment of inertia from spin and gravity data. *Journal of Geophysical Research*, *117*(E12). https://doi.org/10.1029/2012JE004161
McNutt, M. K. (1984). Lithospheric flexure and thermal anomalies. *Journal of Geophysical Research*, *89*(B13), 11180–11194. https://doi.org/10.1029/JB089iB13p11180
Melosh, J., & McKinnon, W. (1988). The tectonics of Mercury. Mercury.
Michel, N. C., Hauck II, S. A., Solomon, S. C., Phillips, R. J., Roberts, J. H., & Zuber, M. T. (2013). Thermal evolution of Mercury as constrained by MESSENGER observations. *Journal of Geophysical Research: Planets*, *118*(5), 1033–1044. https://doi.org/10.1002/jgre.20049
Mueller, S., & Phillips, R. J. (1995). On the reliability of lithospheric constraints derived from models of outer-rise flexure. *Geophysical Journal International*, *123*(3), 887–902. https://doi.org/10.1111/j.1365-246X.1995.tb06896.x
Namur, O., Collinet, M., Charlier, B., Grove, T. L., Holtz, F., & McCammon, C. (2016). Melting processes and mantle sources of lavas on mercury. *Earth and Planetary Science Letters*, *439*, 117–128. https://doi.org/10.1016/j.epsl.2016.01.030
Nimmo, F., & Watters, T. R. (2004). Depth of faulting on Mercury: Implications for heat flux and crustal and effective elastic thickness. *Geophysical Research Letters*, *31*(L02701). https://doi.org/10.1029/2003GL018847
Noyelles, B., Frouard, J., Makarov, V. V., & Efroimsky, M. (2014). Spin–orbit evolution of Mercury revisited. *Icarus*, *241*, 26–44. https://doi.org/10.1016/j.icarus.2014.05.045
Padovan, S., Tosi, N., Plesa, A.-C., & Ruedas, T. (2017). Impact-induced changes in source depth and volume of magmatism on Mercury and their observational signatures. *Nature Communications*, *8*(1), 1945. https://doi.org/10.1038/s41467-017-01692-0
Padovan, S., Wieczorek, M. A., Margot, J.-L., Tosi, N., & Solomon, S. C. (2015). Thickness of the crust of Mercury from geoid-to-topography ratios. *Geophysical Research Letters*, *42*(4), 1029–1038. https://doi.org/10.1002/2014GL062487
Paige, D. A., Siegler, M., Harmon, J., Neumann, G., Mazarico, E., Smith, D., et al. (2012). Thermal stability of volatiles in the north polar region of mercury. *Science*, *339*(6117), 300–303. https://doi.org/10.1126/science.1231106
Paige, D. A., Wood, S. E., & Vasavada, A. R. (1992). The thermal stability of water ice at the poles of mercury. *Science*, *258*(5082), 643–646. https://doi.org/10.1126/science.258.5082.643
Peplowski, P., Lawrence, D., Feldman, W., Goldsten, J., Bazell, D., Evans, L., et al. (2015). Geochemical terranes of Mercury's northern hemisphere as revealed by MESSENGER neutron measurements. *Icarus*, *253*, 346–363. https://doi.org/10.1016/j.icarus.2015.02.002
Peterson, G. A., Johnson, C. L., & Jellinek, A. M. (2021). Thermal evolution of Mercury with a volcanic heat-pipe flux: Reconciling early volcanism, tectonism, and magnetism. *Science Advances*, *7*(40), eabh2482. https://doi.org/10.1126/sciadv.abh2482
Phillips, R., Byrne, P., James, P. B., Mazarico, E., Neumann, G. A., & Perry, M. E. (2018). *Mercury's crust and lithosphere: Structure and mechanics*. In S. Solomon, L. Nittler, & B. Anderson (Eds.), 52–84. https://doi.org/10.1017/9781316650684.004

Plesa, A.-C., Grott, M., Tosi, N., Breuer, D., Spohn, T., & Wieczorek, M. A. (2016). How large are present-day heat flux variations across the surface of Mars? *Journal of Geophysical Research*, *121*(12), 2386–2403. https://doi.org/10.1002/2016JE005126

Plesa, A.-C., Padovan, S., Tosi, N., Breuer, D., Grott, M., Wieczorek, M. A., et al. (2018). The thermal state and interior structure of mars. *Geophysical Research Letters*, *45*(22), 12198–12209. https://doi.org/10.1029/2018GL080728

Plesa, A. C., Tosi, N., Grott, M., & Breuer, D. (2015). Thermal evolution and urey ratio of mars. *Journal of Geophysical Research: Planets*, *120*(5), 995–1010. https://doi.org/10.1002/2014JE004748

Rovira-Navarro, M., Matsuyama, I., & Berne, A. (2024). A spectral method to compute the tides of laterally heterogeneous bodies. *Planet. Science Journal*, *5*(5), 129. https://doi.org/10.3847/PSJ/ad381f

Schubert, G., Turcotte, D. L., & Olson, P. (2001). *Mantle convection in the Earth and planets*. Cambridge University Press.

Siegler, M. A., Bills, B. G., & Paige, D. (2013). Orbital eccentricity driven temperature variation at Mercury's poles. *Journal of Geophysical Research: Planets*, *118*(5), 930–937. https://doi.org/10.1002/jgre.20070

Smith, D. E., Zuber, M. T., Phillips, R. J., Solomon, S. C., Hauck, S. A., Lemoine, F. G., et al. (2012). Gravity field and internal structure of Mercury from MESSENGER. *Science*, *336*(6078), 214–217. https://doi.org/10.1126/science.1218809

Sori, M. M. (2018). A thin, dense crust for Mercury. *Earth and Planetary Science Letters*, *489*, 92–99. https://doi.org/10.1016/j.epsl.2018.02.033

Stevenson, D. J., Spohn, T., & Schubert, G. (1983). Magnetism and thermal evolution of the terrestrial planets. *Icarus*, *54*(3), 466–489. https://doi.org/10.1016/0019-1035(83)90241-5

Tian, Z., Zuber, M., & Stanley, S. (2015). Magnetic field modeling for mercury using dynamo models with a stable layer and laterally variable heat flux. *Icarus*, *260*, 263–268. https://doi.org/10.1016/j.icarus.2015.07.019

Tosi, N., Čadek, O., Běhounková, M., Káňová, M., Plesa, A.-C., Grott, M., et al. (2015). Mercury's low-degree geoid and topography controlled by insolation-driven elastic deformation. *Geophysical Research Letters*, *42*(18), 7327–7335. https://doi.org/10.1002/2015GL065314

Tosi, N., Grott, M., Plesa, A.-C., & Breuer, D. (2013). Thermo-chemical evolution of Mercury's interior. *J. Geophys. Res. (Planets).*, *118*(12), 2474–2487. https://doi.org/10.1002/jgre.20168

Tosi, N., & Padovan, S. (2021). Mercury, moon, mars: Surface expressions of mantle convection and interior evolution of stagnant-lid bodies. In S. C. H. M. M. Ballmer & J. Konter (Eds.), *Mantle convection and surface expressions (chap. 17)*. AGU. https://doi.org/10.1002/9781119528609.ch17

van Zelst, I., Crameri, F., Pusok, A. E., Glerum, A., Dannberg, J., & Thieulot, C. (2022). 101 geodynamic modelling: How to design, interpret, and communicate numerical studies of the solid earth. *Solid Earth*, *13*(3), 583–637. https://doi.org/10.5194/se-13-583-2022

Vasavada, A. R., Paige, D. A., & Wood, S. E. (1999). Near-surface temperatures on mercury and the moon and the stability of polar ice deposits. *Icarus*, *141*(2), 179–193. https://doi.org/10.1006/icar.1999.6175

Wang, Y., Xiao, Z., & Xu, R. (2022). Multiple mantle sources of high-magnesium terranes on mercury. *Journal of Geophysical Research: Planets*, *127*(5), e2022JE007218. https://doi.org/10.1029/2022JE007218

Watters, T. R., Schultz, R. A., Robinson, M. S., & Cook, A. C. (2002). The mechanical and thermal structure of mercury's early lithosphere. *Geophysical Research Letters*, *29*(11), 1–4. https://doi.org/10.1029/2001GL014308

Weider, S. Z., Nittler, L. R., Starr, R. D., Crapster-Pregont, E. J., Peplowski, P. N., Denevi, B. W., et al. (2015). Evidence for geochemical terranes on Mercury: Global mapping of major elements with MESSENGER's X-Ray Spectrometer. *Earth and Planetary Science Letters*, *416*, 109–120. https://doi.org/10.1016/j.epsl.2015.01.023

Wieczorek, M. A., Correia, A. C. M., Le Feuvre, M., Laskar, J., & Rambaux, N. (2012). Mercury's spin-orbit resonance explained by initial retrograde and subsequent synchronous rotation. *Nature Geoscience*, *5*(1), 18–21. https://doi.org/10.1038/ngeo1350

Wieczorek, M. A., & Meschede, M. (2018). SHTools: Tools for working with spherical harmonics. *Geochemistry, Geophysics, Geosystems*, *19*(8), 2574–2592. https://doi.org/10.1029/2018gc007529

Williams, J. P., Ruiz, J., Rosenburg, M. A., Aharonson, O., & Phillips, R. J. (2011). Insolation driven variations of Mercury's lithospheric strength. *Journal of Geophysical Research*, *116*(E01008), E01008. https://doi.org/10.1029/2010JE003655

Zuber, M., Smith, D., Phillips, R., Solomon, S., Neumann, G., Hauck, S., et al. (2012). Topography of the northern hemisphere of Mercury from MESSENGER laser altimetry. *Science*, *336*(6078), 217–220. https://doi.org/10.1126/science.1218805